References

[1] Gaspers, P. A., Jr., "Applications of Recent Panel Flutter Research to Space Shuttle. Part I—Boundary Layer and Hypersonic Effects," *NASA Space Shuttle and Technology Conference, Vol. III—Dynamics and Aeroelasticity*, TM X-2274, 1971, NASA, pp. 247–264.

[2] Bohon, H. L. and Shore, C. P., "Applications of Recent Panel Flutter Research to Space Shuttle. Part II—Influence of Edge Clips and Flow Angularity," TM X-2274, March 1971, NASA, pp. 247–264.

[3] Leissa, A., *Vibration of Plates*, NASA SP-160, 1969.

[4] Dowell, E. H., "Free Vibrations of a Linear Structure with Arbitrary Support Conditions," *Journal of Applied Mechanics*, Vol. 38. No. 3, Sept. 1971, pp. 595–600.

[5] Dowell, E. H., "Free Vibrations of an Arbitrary Structure in Terms of Component Modes," *Journal of Applied Mechanics*, Vol. 39, No. 3, Sept. 1972, pp. 727–732.

[6] Dowell, E. H., "Noise or Flutter or Both?" *Journal of Sound and Vibration*, Vol. 11, No. 2, 1970, pp. 159–180.

[7] Dowell, E. H., "Panel Flutter: A Review of the Aeroelastic Stability of Plates and Shells," *AIAA Journal*, Vol. 8, No. 3, March 1970, pp. 385–399.

[8] Dowell, E. H., "Generalized Aerodynamic Forces on a Plate Undergoing Transient Motion in a Shear Flow with an Application to Panel Flutter," *AIAA Journal*, Vol. 9, No. 5, May 1971, pp. 834–841.

[9] Washizu, K., *Variational Methods in Elasticity and Plasticity*, Pergamon Press, New York, 1968, pp. 163–165.

[10] Bisplinghoff, R. L., Ashley, H., and Halfman, R., *Aeroelasticity*, Addison-Wesley, Reading, Mass., 1955.

[11] Gaspers, P. A., Jr. and Redd, B., "A Theoretical Analysis of the Flutter of Orthotropic Panels Exposed to a High Supersonic Stream of Arbitrary Direction," TN D-3551, 1966, NASA.

[12] Stroud, W. J., "Elastic Constants for Bending and Twisting of Corrugation-Stiffened Panels," TR-166, 1963, NASA.

[13] Dowell, E. H., "Flutter of Multibay Panels at High Supersonic Speeds," *AIAA Journal*, Vol. 2, No. 10, Oct. 1964, pp. 1805–1811

JUNE 1973 J. SPACECRAFT VOL. 10, NO. 6

A Theoretical and Experimental Study of a Jet Stretcher System

R. C. BAUER,* E. H. MATKINS,† R. L. BAREBO,† AND W. C. ARMSTRONG‡

ARO Inc. Arnold Air Force Station, Tenn.

Analytical techniques were developed for estimating diffuser performance, and for evaluating the feasibility of using an axisymmetric jet stretcher for angle-of-attack testing. Diffuser starting limits are imposed by : 1) nozzle exit boundary layer, 2) blockage area, and 3) jet stretcher ambient pressure level. The diffuser analysis estimates the starting conditions limited by either the nozzle exit boundary layer or the jet stretcher ambient pressure level. Experimental results show the analysis for diffuser starting conditions to be conservative and accurate to within 10% for engine-off operation. The feasibility of using an axisymmetric jet stretcher for angle-of-attack testing was determined by establishing a criteria for acceptable jet stretcher performance based on maintaining the static pressure distribution on the test body to within ± 10% of the interference free pressure distribution. A local application of linearized theory was used to determine the proper position of the jet stretcher and to indicate the regions that require bleed flow. The analysis was applied to a small-scale jet stretcher system for test body angles of attack of 4° and 8°. Experimental results verified the analysis and showed that the maximum possible off-design angle of attack of the test body is about 5.0°

Nomenclature

A = area
C_p = model pressure coefficient
cp = specific heat at constant pressure
F = stream thrust plus pressure force
F_s = total drag force
L = diffuser gap, see Fig. 1
l = length of cylindrical diffuser, see Fig. 1
M = Mach number
m = mass flow
p = static pressure
q = dynamic pressure
r_N = radius of nozzle exit
r_j = radius of jet stretcher inlet
T = static temperature
X_B = distance from nose of test body along its centerline
X_F = feedback distance
X_{FA} = allowable feedback distance, see Fig. 3
X_{js} = distance from nozzle exit to jet stretcher inlet, see Fig. 3
X_j = distance from jet stretcher inlet along its centerline
α_B = angle of test body relative to nozzle centerline; angle of attack, see Fig. 14
α_j = angle of jet stretcher relative to nozzle centerline, see Fig. 14
β = mismatch angle between jet stretcher surface and the interference free flowfield, deg, see Fig. 14
γ = ratio of specific heats
δ_N = total boundary-layer thickness at nozzle exit
θ = radial angle measured from leeward side of test body, deg
λ = blockage ratio—open area between inlets to annular area upstream of inlets
μ = Mach angle

Subscripts

B = diffuser exit, see Fig. 1
BLS = Boundary-layer separation

Received September 12, 1972; presented as Paper 72–1024 at the AIAA 7th Aerodynamic Testing Conference, Palo Alto, Calif., September 13–15, 1972; revision received February 5, 1973. This research was supported by the Arnold Engineering Development Center, under sponsorship of the Aerospace Propulsion Laboratory.

Index category: Airbreathing Engine Testing.

* Research Engineer. Member AIAA.

† Project Engineer.

‡ Scientist.

b = base region
C = chamber region, see Fig. 1
E = external region, see Fig. 1
i = engine inlet on test body
j = radial gap between nozzle exit and jet stretcher inlet
N = nozzle
p = jet stretcher porous wall, see Fig. 1
S = starting conditions
t = total or stagnation condition
1 = test body engine, see Fig. 1
2 = region between test body and jet stretcher, see Fig. 1
3 = diffuser gap region, see Fig. 1

Superscript

* = throat region

I. Introduction

A NEW Aerodynamic and Propulsion Test unit (APTU) is being constructed at AEDC to test ramjet engines which operate at supersonic Mach numbers and low altitudes. Many of these tests will utilize the jet stretcher concept, and the diffuser will consist of a cylindrical duct, which connects to a larger duct and exhausts to the atmosphere. The diameter of the diffuser will be selected to allow the system to be self-starting over a range of simulated altitudes.

The jet stretcher (or jet extender, as it has been called by some) is basically an aerodynamically tailored device which replaces a known streamline or stream surface in the flow about the test vehicle with a boundary-layer corrected wall or shroud, and provides proper flow at the engine inlets (Fig. 1). To accomplish this, the jet stretcher must be positioned aft of the bow shock generated by the forebody nose and forward of any expansion or compression waves generated at the nozzle exit to prevent external disturbances from influencing the pressures on the test model and in the surrounding flowfield.

The requirement for testing the inlet and engine as a complete system is necessary in many missile and air-frame configurations because of the strong aerodynamic coupling between the forebody and inlets which influence the over-all engine performance. At zero angle of attack it is possible through proper nozzle design to simulate the flow approaching an aft-mounted inlet by letting the test vehicle forebody become the centerbody of the test nozzle, or it may be possible to test the inlet-engine system without the forebody by designing the approaching air passages to simulate the inlet flow. Unfortunately, neither of these approaches is adequate for meeting the requirement for testing multiple inlet configurations at finite angles of attack. The possibility of using an axisymmetric jet stretcher for angle-of-attack testing was indicated in Ref. 1 although the primary objective of that study was to verify the jet stretcher concept for zero angle-of-attack testing.

In this paper, the results of a study of both jet stretcher diffuser performance and the feasibility of using an axisymmetric jet stretcher for angle-of-attack testing are presented.

II. Diffuser Analysis

The analysis is divided into two parts, general performance and starting conditions. The general performance analysis determines the relationship between the nozzle total pressure p_{t_N}, the chamber pressure p_c, and the exhaust pressure p_B. The starting conditions analysis relates the nozzle total pressure p_{t_N} to the maximum chamber pressure $(p_c)_s$ at which the system will operate in a steady-state, started (defined in Sec. IIB) condition. Combining these two analyses relates the nozzle total pressure p_{t_N} to the maximum exhaust pressure $(p_B)_s$ at which the system will operate in its started condition. A detailed development of each analysis is presented in the following sections.

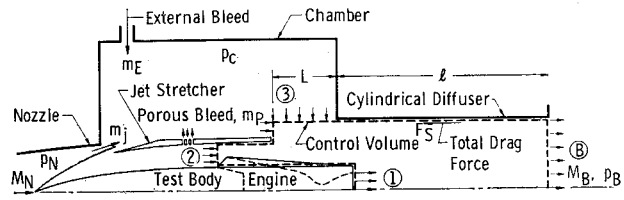

Fig. 1 Sketch of jet stretcher diffuser system.

A. General Performance Analysis

The equations describing the general performance of a jet stretcher diffuser system are derived by applying the fluid mechanical conservation laws to the control volume shown in Fig. 1. The conservation laws are applied based on the following assumptions: 1) $\alpha_B = 0$. 2) Since test body engine inlets are located at least five body diameters from the nose, the flow conditions on the control volume surface 2 are one dimensional. 3) The engine exhaust is one dimensional. 4) The jet stretcher is cylindrical beyond the engine inlets. 5) Flow conditions over surface 3 of the control volume are uniform. 6) The static pressure on the blunt base of the jet stretcher and on surface 3 of the control volume are equal. 7) The cylindrical diffuser is of sufficient length to allow complete mixing. Therefore, the flow conditions at the diffuser exit (surface B of the control volume) are one-dimensional. 8) All gases are perfect. 9) The chamber pressure p_c is the total pressure of the flow on surface 3 of the control volume. 10) There is no afterburning of the engine exhaust. 11) The nozzle and jet stretcher are flowing full. Based on these assumptions, the basic equations are:

Conservation of Mass Flow

$$m_1 - m_i + m_2 + m_3 = m_B \tag{1}$$

Conservation of Momentum (X direction)

$$F_1 + P_{b1} A_{b1} - F_i + F_2 + P_3 A_{b3} + F_3 - F_s = F_B \tag{2}$$

Conservation of Energy

$$m_3 C_{p3} T_{t3} = m_j C_{pj} T_{tj} + m_p C_{pp} T_{tp} + m_E C_{pE} T_{tE} \tag{3}$$

$$m_B C_{pB} T_{tB} = m_1 C_{p1} T_{t1} + (m_2 - m_i) C_{p2} T_{t2} + m_3 C_{p3} T_{t3} \tag{4}$$

In practice, limitations to this analysis are imposed by boundary-layer separation and choking phenomena. Assumption 11 is only valid if the ratio of chamber pressure p_c to nozzle exit pressure p_N and jet stretcher exit pressure does not exceed the corresponding allowable boundary-layer separation pressure ratios. This determines the maximum chamber pressure at which both the nozzle and jet stretcher will flow full. The minimum chamber pressure p_c is determined by the occurrence of diffuser choking at either its entrance (surface 3 in Fig. 1), exit (surface B in Fig. 1), or internally. The analysis can predict the occurrence of choking on control volume surfaces 3 and B. However, internal diffuser choking is caused by the pluming of the flow from the jet stretcher exit, thus causing a constriction within the diffuser. This pluming occurs when the static pressure on control volume surface 3 is less than the static pressure at the jet stretcher exit. A conservative estimate (minimum p_c greater than experiment) of internal diffuser choking is made by assuming that choking occurs when the static pressure p_3 equals the static pressure at the jet stretcher exit. This is a good estimate for diffuser systems of practical interest since the diffuser diameter is not much larger than the jet stretcher exit diameter and very little pluming is required for internal diffuser choking to occur. An accurate estimate of internal diffuser choking can be made by computing the plume shape using the well-known method of characteristics solution technique.

The complete range of applicability of this analysis can be represented as follows:

$$p_c/p_N \leq (p_c/p_N)_{BLS} \quad (5)$$

$$M_3 \leq 1.0 \quad (6)$$

$$M_B \leq 1.0 \quad (7)$$

$$(p_3/p_2)_{BLS} \geq p_3/p_2 \geq 1.0 \quad (8)$$

In the last condition, the pressure p_2 (static pressure on control volume surface 2) is taken to be the jet stretcher exit static pressure since the flow conditions on control volume surface 2 are assumed to be one-dimensional and the jet stretcher has constant area beyond surface 2. However, this assumption is only valid if the jet stretcher is terminated upstream of the engine inlets.

B. Starting Conditions Analysis

A jet stretcher diffuser system is defined to be operating in a started conditon when there are no disturbances from the nozzle and jet stretcher exits influencing the test body flowfield of interest.

These disturbances occur when: 1) The nozzle exit boundary layer thickness is greater than the radial distance between the nozzle exit and the jet stretcher inlet. 2) The blockage between the test body and jet stretcher exceeds the normal shock limit. 3) The chamber pressure p_c is different from the nozzle and jet stretcher exit static pressures.

Disturbance sources 1 and 2, for most configurations, can be eliminated by properly designing the jet stretcher for blockage and the range of test Reynolds numbers of interest. There is a minimum nozzle Reynolds number below which it is impossible to start a given jet stretcher diffuser system. This minimum Reynolds number can be conservatively estimated (greater than experiment) by assuming it is that Reynolds number which produces a nozzle exit boundary equal in thickness to the radial distance between the nozzle exit and the jet stretcher inlet. The nozzle exit boundary layer can be computed for various Reynolds numbers by the method presented in Ref. 2. Disturbance source 3 is eliminated by reducing the chamber pressure p_c to a sufficiently low level for starting. The following analysis estimates the maximum chamber pressure p_c at which a given jet stretcher system will operate in a started condition, assuming disturbance sources 1 and 2 have been eliminated.

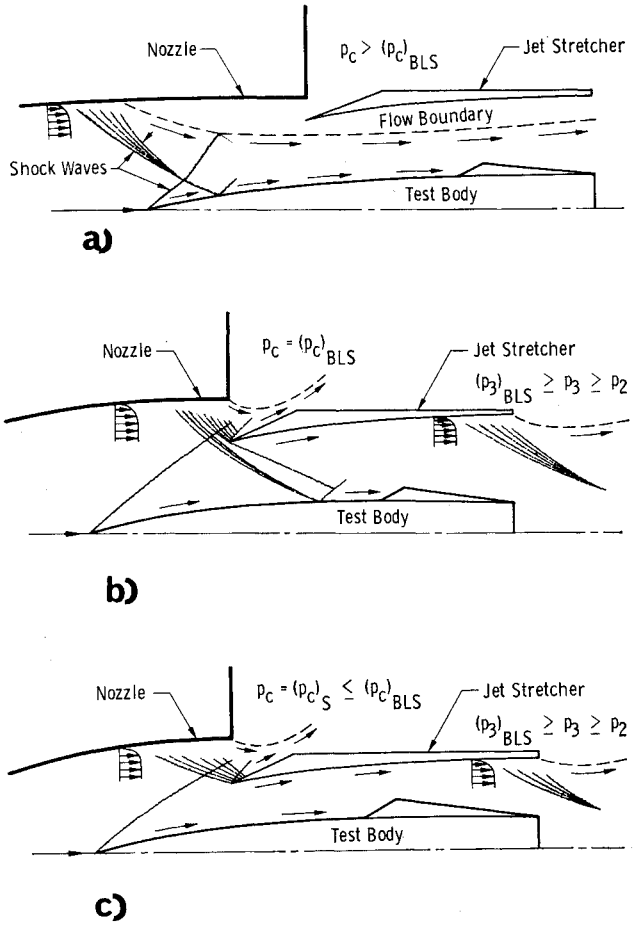

Fig. 2 Flow conditions during the starting process; a) system unstarted; b) nozzle and jet stretcher flowing full, system unstarted; c) system started.

Consider a steady-state starting process produced by imposing various over-all pressure ratios p_B/p_{t_N} to the system shown in Fig. 1. The different types of flow conditions that will exist are shown in Fig. 2. An unstarted flowfield (Fig. 2a) exists when the chamber pressure p_c is greater than the maximum allowable chamber pressure $(p_c)_{BLS}$ required for the boundary layer to be attached at the nozzle exit. At some point in the steady-state starting process, the chamber pressure p_c will become equal to this maximum allowable chamber pressure $(p_c)_{BLS}$ and the flowfield will be as shown in Fig. 2b. Although both the nozzle and jet stretcher are flowing full, the system is unstarted because of the upstream feedback of the chamber pressure p_c in the nozzle boundary layer. This high-pressure feedback produces compression waves which are not entirely intercepted by the jet stretcher, thus causing a disturbance on the test body. For the system to be started, all of the compression waves produced by the high-pressure feedback must be intercepted by the jet stretcher as shown in Fig. 2c. This will occur at a chamber pressure that is less than the maximum allowable chamber pressure.

To quantitatively determine the chamber pressure $(p_c)_s$ for starting, it is necessary to analytically represent: a) boundary-layer separation pressure ratio, b) high-pressure feedback in a boundary layer, and c) allowable high-pressure distance in the nozzle boundary layer. Simple analytical expressions for each phenomena are developed in the following sections.

1. *Boundary-layer separation pressure ratio*

The boundary layers considered are at the nozzle and jet stretcher exits. These boundary layers are usually fully turbulent (at high Reynolds number) in the Mach number range 2.0 to 4.0. A compilation of experimental data by Schulz[3] resulted in the following simple relationships for the boundary-layer separation pressure ratios at the nozzle and jet stretcher exits.

$$(p_c/p_N)_{BLS} = M_N \quad (9)$$

$$(p_3/p_2)_{BLS} = M_2 \quad (10)$$

2. *High-pressure feedback in a turbulent boundary layer*

The boundary layers experiencing an adverse pressure are at the nozzle and jet stretcher exits. A detailed calculation of this flow process is not necessary since only the extent of the feedback as a function of pressure ratio is required in the Starting Conditions Analysis. A linear relationship is assumed, established by the following assumptions: a) Extent of feedback is scaled by the boundary-layer thickness,[4] δ_N. b) At the boundary-layer separation pressure ratio, the feedback distance is five boundary-layer thicknesses.[4] c) For equal pressures ($p_c = p_N$), the feedback distance is zero.

Based on these assumptions, the linear relation for feedback distance at the nozzle exit is given by the following equation

$$p_c/p_N = 1 + \tfrac{1}{5}[(p_c/p_N)_{BLS} - 1]X_F/\delta_N \quad (11)$$

3. *Allowable feedback distance*

The allowable feedback distance is the maximum distance upstream of the nozzle exit at which disturbances can originate

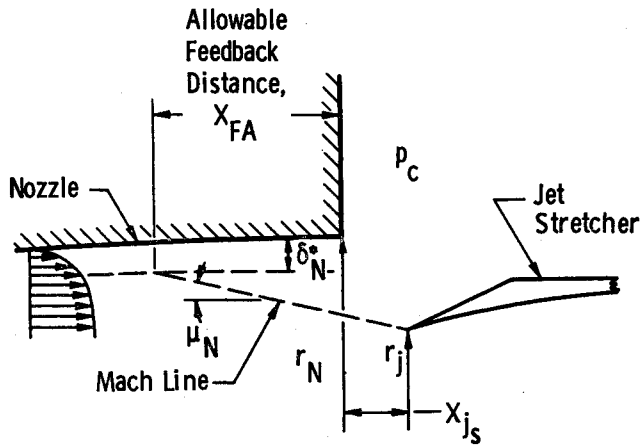

Fig. 3 Allowable feedback distance.

and still be intercepted by the jet stretcher. This distance can be estimated by geometry from Fig. 3. The equation is

$$\frac{X_{FA}}{r_N} = (M_N^2 - 1)^{\frac{1}{2}}\left[1 - \frac{r_j}{r_N} - \frac{\delta_N^*}{r_N}\right] - \frac{X_{js}}{r_N} \qquad (12)$$

The maximum chamber pressure $(p_c)_s$ at which a given jet stretcher diffuser system will start is that which produces a feedback distance X_F equal to the allowable feedback distance X_{FA}. Using this condition, it is possible to combine Eqs. (9, 11, and 12) yielding

$$\frac{p_c}{p_{Ns}} = \frac{M_N - 1}{5\delta_N/r_N}\left[\left(1 - \frac{r_j}{r_N} - \frac{\delta_N^*}{r_N}\right)(M_N^2 - 1)^{\frac{1}{2}} - \frac{X_{js}}{r_N}\right] + 1 \qquad (13)$$

This equation applies in the following range

$$M_N \geq (p_c/p_N)_s \geq 1.0 \qquad (14)$$

For $(p_c/p_N)_s > M_N$ the starting value is

$$(p_c/p_N)_s = M_N \qquad (15)$$

For $(p_c/p_N)_s < 1.0$, the system will not start since the allowable feedback distance X_{FA} is less than zero.

C. Over-All Starting Pressure Ratio

The over-all starting pressure ratio $(p_B)_s/p_{tN}$ is determined by combining the General Performance Analysis with the Starting Conditions analysis previously described. The detailed equations were programmed in Fortran IV and the solutions were obtained with an IBM 370/155 computer.

III. Experimental Diffuser Study

A. Objective

The purpose of this study was to provide experimental data for evaluation of the analysis. In particular, it was of interest to establish the accuracy of the predicted starting conditions, and to determine if a diffuser length of 5 diam is sufficient to achieve complete mixing.

B. Experimental Apparatus

A sketch of the experimental apparatus is presented in Fig. 4. This is the same apparatus used in the study reported in Ref. 5 with the jet stretcher inlet machined back 0.16 in. to eliminate a fabrication error. The apparatus consists of an 8-in.-exit-diam, Mach number 3.04 nozzle; a 3.5-in.-diam test body with a 2.92 von Kármán forebody, a jet stretcher, and a 12-in.-diam cylindrical diffuser. The nozzle and jet stretcher were corrected for boundary layer based on a nozzle inlet

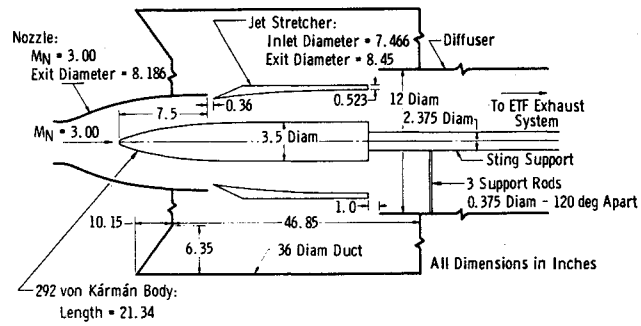

Fig. 4 Experimental jet stretcher diffuser system.

total pressure of 30 psia and a total temperature of 560°R.

Two 12-in.-diam cylindrical diffusers having length to diameter ratios (l/d) of 2.5 and 5.0 were tested. The performance of the l/d = 5.0 diffuser was of primary importance since it is similar to the diffuser to be used in the full-scale APTU currently being constructed at AEDC.

C. Experimental Procedure

1. *Procedure I*

The nozzle total pressure p_{tN} was held constant at 30 psia while the exhaust pressure p_B was first increased from ≈0.6 psia to ≈4.5 psia and then decreased back to ≈0.6 psia in small increments. Steady-state data were obtained at each exhaust pressure.

Data from this test procedure are for a constant nozzle Reynolds number and will indicate the possible occurrence of hysteresis on starting conditions.

2. *Procedure II*

The exhaust pressure p_B was held constant while the nozzle total pressure p_{tN} was first increased from p_B in small increments then decreased back to p_B. Steady-state data were obtained at each nozzle total pressure level. The data from from this test procedure are for a variable nozzle Reynolds number and will also indicate the possible occurrence of hysteresis on starting conditions.

IV. Evaluation of Diffuser Theory

A. Application of Theory

In the following sections, the experimental configuration is analyzed with respect to each of the disturbance sources discussed earlier.

1. *Nozzle boundary-layer limit*

The minimum nozzle Reynolds number or total pressure (since total temperature is constant) for started operation is that which produces a nozzle exit boundary-layer thickness equal to the radial gap between the nozzle exit and the jet stretcher inlet. For the experimental configuration, the nozzle boundary-layer thickness as a function of nozzle total pressure was computed by Bartz method[2] and the minimum nozzle total pressure for started operation is 12.5 psia.

2. *Blockage limit*

The maximum blockage of the experimental configuration occurs at the jet stretcher inlet, and the physical contraction ratio is 0.813. The maximum allowable contraction ratio based on normal shock wave theory is 0.72, thus, blockage effects should not be present in this configuration.

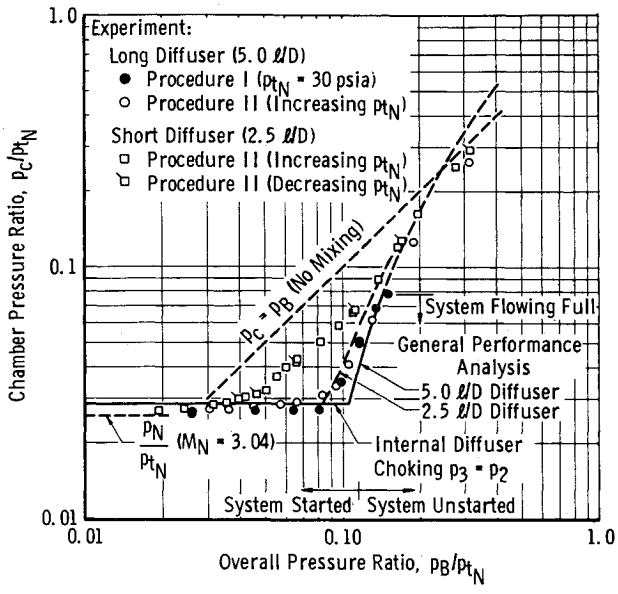

Fig. 5 Effect of diffuser length on general performance.

3. Chamber pressure limit

The major limitation to starting the experimental configuration is that imposed by the chamber pressure. The analysis of this type of starting limitation is applied to the experimental configuration and compared with experiment in the following sections.

B. Comparison of Theory with Experiment

1. Effect of diffuser length

A major assumption in the General Performance Analysis is that the diffuser is of sufficient length to allow complete mixing of the various streams. To evaluate this assumption two diffusers having length-to-diameter ratios of 2.5 and 5.0 were tested. The general performances of these diffusers are compared in Fig. 5, along with the theoretical results. The theory for the short diffuser was modified to account for the 15.45% sting support blockage by assuming isentropic flow through the area change.

The best indicator of the degree of mixing is the recovery ratio p_B/p_c. The maximum recovery pressure ratio for the short diffuser is about 1.6, compared with about 3.0 for the long diffuser. Thus, the short diffuser is not long enough to allow complete mixing. For the long diffuser, the good agreement between theory and experiment indicates that nearly complete mixing is achieved.

2. Effect of diffuser gap

The theory assumes a uniform velocity distribution over a rectangular surface bounding the gap as shown in Fig. 1. Experimental results from the $l/d = 5.0$ diffuser are compared with theory in Fig. 6 for both a zero and 1.0-in. gap. Both the theory and the experiment show the major effect of the gap to be a change in the level of the minimum chamber pressure. According to the theory, the minimum chamber pressure is determined by internal diffuser choking for both gap configurations. For this type of diffuser choking, the theoretical minimum chamber pressure is expected to be greater than experiment as verified in Fig. 9.

3. System start conditions

The Starting Conditions Analysis is based on assumptions concerning turbulent boundary-layer separation pressure ratio, high-pressure feedback in a turbulent boundary layer, and allowable high-pressure feedback distance. No attempt was made to experimentally verify each of these assumptions since only the started conditions are of primary importance.

The theoretical maximum exhaust pressure $(p_B)_s$ required to start the experimental configuration for the test range of nozzle total-pressure levels is compared with experiment in Fig. 7. The experimental start conditions were determined from the measured pressure distribution on the test model. The jet-stretcher-diffuser system is defined to be started when there are no interference effects greater than $\pm 10\%$ of the accepted started static pressure distribution on the test model. The accepted started model pressure distribution may differ from the true interference-free pressure distribution because of improper geometry of the nozzle or jet stretcher or both. Experimental test model pressure coefficient distributions are presented in Figs. 8a and b for test Procedures I and II. The experimental data obtained by test Procedure I (Figs. 7 and 8a) show $(p_B)_s$ required for starting, to be in the range of 3.48–3.98 psia. The corresponding over-all pressure ratios p_B/p_{t_N} are 0.116 and 0.133. The theoretical values are: $(p_B)_s = 3.42$ psia and $(p_B)_s/p_{t_N} = 0.114$, which are about 10% lower than experiment.

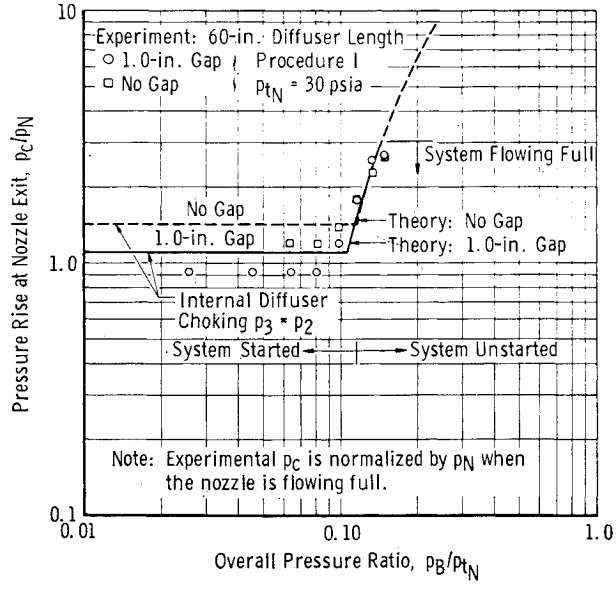

Fig. 6 Effect of diffuser gap on performance.

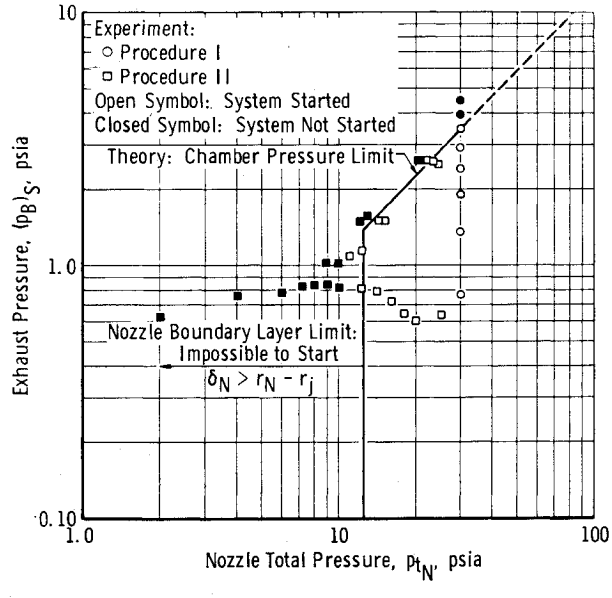

Fig. 7 Comparison of theoretical start conditions with experiment.

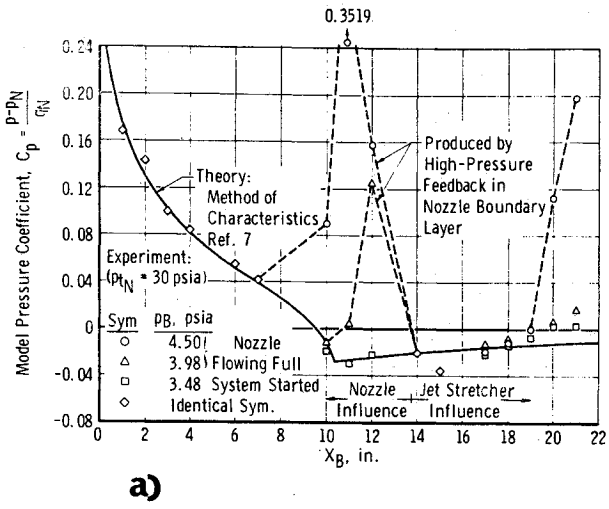

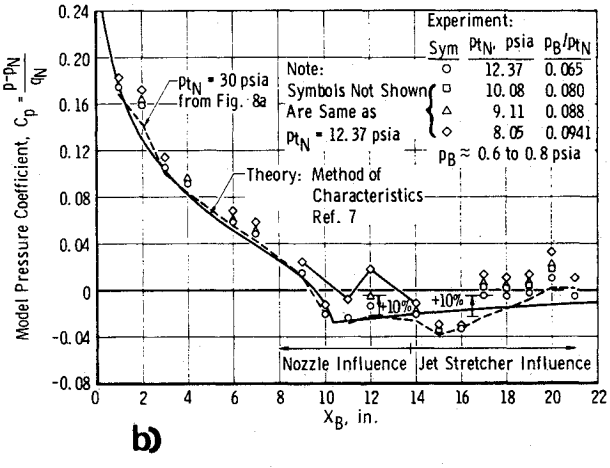

Fig. 8 Static pressure distribution on test body; a) Procedure I; b) Procedure II.

The experimental data from test Procedure II (Figs. 7 and 8b) obtained at the lowest exhaust pressure ($p_B \approx 0.6$ psia) show that the starting conditions were determined by the nozzle boundary-layer limit rather than the chamber pressure limit. Therefore, the experimental data determine the minimum nozzle total pressure (or Reynolds Number) for starting. The experimental results presented in Fig. 8b show the minimum nozzle total pressure for starting to be 12.37 psia. The theoretical value of 12.5 psia is about 2% greater than experiment.

4. *Hysteresis effects*

A hysteresis effect on starting conditions means the over-all pressure ratio p_B/p_{tN} required for starting the system is less than that required to unstart the system. Usually hysteresis effects are caused by relatively high blockage. The blockage ratio for the test configuration is 0.813 compared with an allowable blockage ratio of 0.72, and the experimental results show no hysteresis effect on starting conditions.

C. Effects of Test Body Angle of Attack and Simulated Engine Inlets

It is anticipated that certain full-scale tests will have the test body at a finite angle of attack and it will be necessary to establish the interference-free flowfield before the ramjet engine can be operated. Both test body angle of attack and closed engine inlets increase the complexity of the flowfield to such an extent it is usually impossible to analytically predict their effect on diffuser performance. As a result, it is necessary to define these effects experimentally. This was done for the

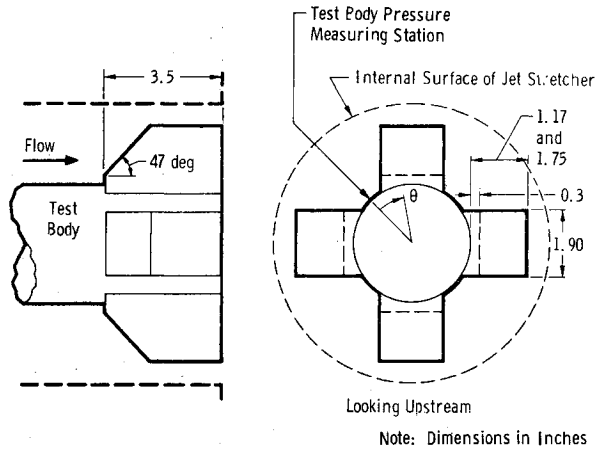

Fig. 9 Sketch of simulated engine inlets.

experimental configuration previously described for a test body angle of attack of 8° and with the addition of the simulated engine inlets shown in Fig. 9. Two sets of inlets were used having blockage ratios, λ of 0.809 and 0.714. These inlets are unrealistically large compared with the test body in order to provide a significant blockage in this test apparatus. The blockage ratio of the large inlets exceeds the allowable ratio of 0.72 and so it should not be possible to start this configuration.

1. *Angle-of-attack effect*

Experimental results with the test body at 8° angle of attack are compared with the zero angle of attack results in Fig. 10. These results show two effects on diffuser performance because of test body angle of attack. The first is an undesirable change in the general performance curve, perhaps caused by the diffuser length being too short to allow a complete reacceleration of the test body wake. The second is a significant increase in the minimum chamber pressure because of internal diffuser choking. It will be shown in the next section that this high-chamber pressure prevents the system from ever becoming started.

2. *Effect of simulated engine inlets*

Two of the small inlets were added to the test body in the 8° angle-of-attack test configuration and the experimental diffuser performance is presented in Fig. 10. These results show

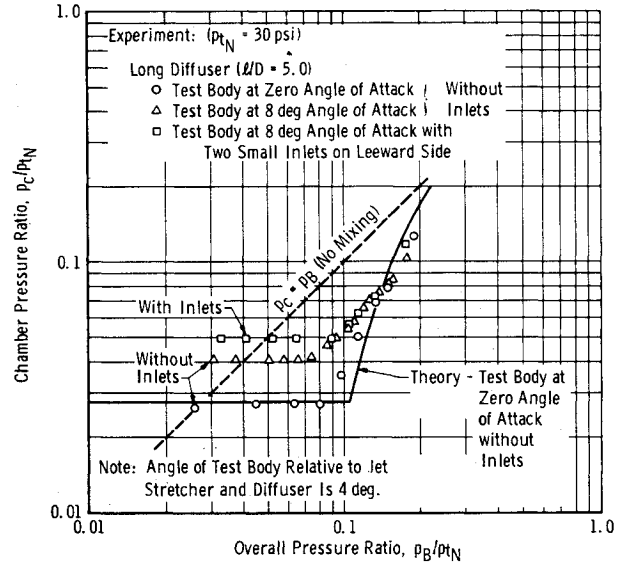

Fig. 10 Effects of test body angle of attack and simulated engine inlets on diffuser performance.

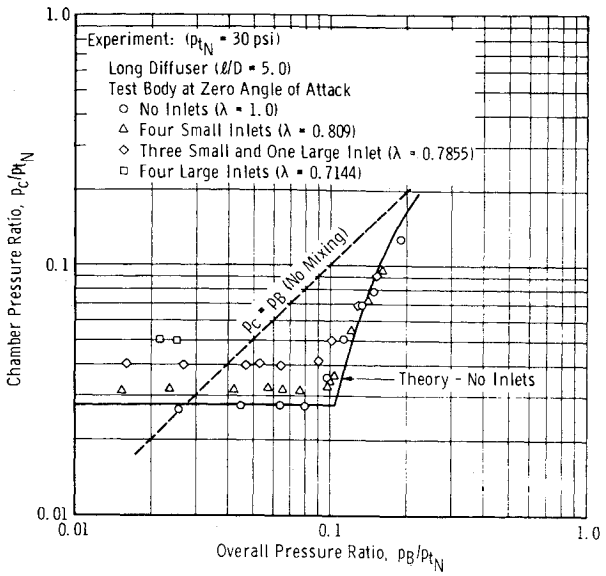

Fig. 11 Effect of simulated engine inlets on diffuser performance.

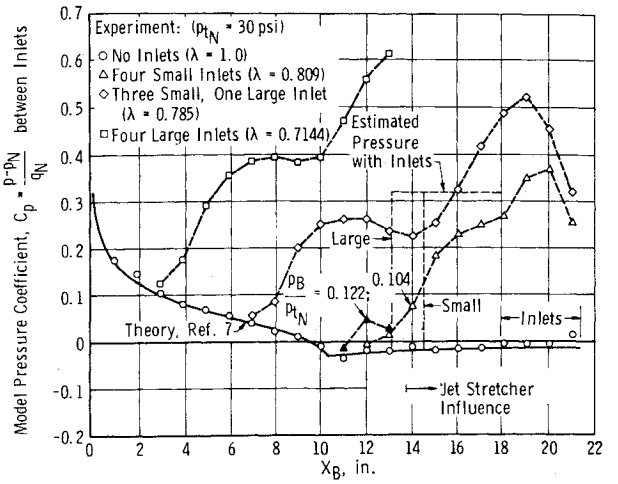

Fig. 13 Effect of simulated inlets on test body pressure distribution at zero angle of attack.

that only diffuser choking is affected by the simulated inlets. Apparently the simulated inlets, like test body angle of attack, increase the average jet stretcher exit pressure causing internal diffuser choking to occur at a relatively high chamber pressure.

The effect of simulated inlets on diffuser performance with the test body at zero angle of attack is presented in Fig. 11. Again, the major effect of the simulated inlets is to increase the chamber pressure at which choking occurs caused by an increase in the average jet stretcher exit pressure. The major aerodynamic features of the flowfield for the test configuration having four small inlets is presented in Fig. 12. The flowfield over the inlet was estimated by assuming the inlet acts like a two-dimensional forward facing step and the pressure in the separated region is that required to separate the boundary layer. This simple analysis shows that if supersonic flow is established inside the jet stretcher, then the influence of the small inlets on the test body pressure distribution begins at station 14.5 in. For the large inlets, the influence begins at station 13.1 in. In Fig. 13, experimental pressure distributions measured on the test body between inlets are compared for the various inlet configurations. The jet stretcher is shown to be operating properly by the results for the test configuration without inlets. With four small inlets ($\lambda = 0.809$) the experimental results are in close enough agreement with the simple analysis to conclude that the flow conditions approaching the entrance to each inlet is properly simulated. The over all pressure ratio p_B/p_t required for starting is shown to be in the range 0.104 and 0.122 which is the same as that required for starting the system without simulated inlets. With four large inlets ($\lambda = 0.7144$) the experimental results are greatly

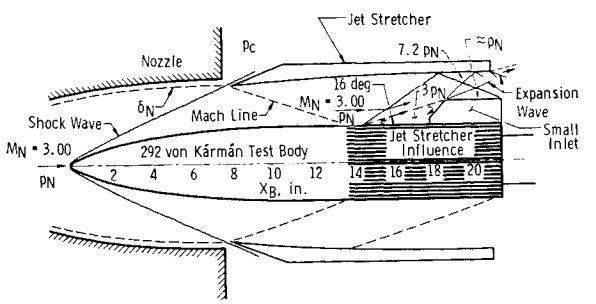

Fig. 12 Test configuration at zero angle of attack with simulated engine inlets.

different from the simple analysis because of blockage effects. This was expected since the limiting blockage ratio is 0.72. The experimental results with three small and one large inlet were unexpected since the average blockage ratio is 0.785. However, the measurements presented were made along the edge of the quadrant containing the one large inlet so that it is possible for the flow conditions approaching the opposite two small inlets to be properly simulated.

3. *Hysteresis Effects*

The experiments described in this section were conducted by maintaining the nozzle total pressure at 30 psi and varying the exhaust pressure (Procedure I). This test procedure did not reveal a hysteresis effect for any of the configurations tested.

V. Jet Stretcher Performance

Previous jet stretcher studies were primarily concerned with verification of the jet stretcher concept for zero angle-of-attack testing. In this section, the feasibility of the jet stretcher concept for finite angle-of-attack testing is discussed.

A. Analysis

The testing of an axisymmetric vehicle at zero angle of attack requires an axisymmetric jet stretcher. To test this same vehicle at a finite angle of attack requires a jet stretcher having an unsymmetrical three-dimensional internal suface. Since the fabrication of such a surface is impractical at the present time, only axisymmetric or simply modified axisymmetric jet stretchers are of practical interest. The possibility of using an axisymmetric jet stretcher for angle-of-attack testing has been indicated by experimental results.[5] These results show that for a finite angle of attack of the test vehicle with the jet stretcher at zero angle of attack, major disturbances originate from the top (leeward side of test vehicle) and bottom (windward side of test vehicle) regions of the jet stretcher while the sides remain acceptably matched to the interference-free flowfield. In addition, these disturbances result from opposite processes, i.e., expansion from the top and compression from the bottom, thus indicating that the disturbances can be reduced or eliminated by simply pitching the jet stretcher to an angle of attack. Intuitively, the remaining disturbances, if any, could be further reduced by bleed flow through selected porous regions on the jet stretcher surface. This combination of pitching the jet stretcher and the use of bleed flow is the approach followed in this study.

To use a jet stretcher, designed for a test body at zero angle of attack, and a given Mach number, at finite angle of attack (off-design condition) requires the establishment of a criterion for acceptable jet stretcher performance that is consistent with the test objectives. To test an engine in a vehicle requires a simulation of the forebody aerodynamics sufficient to allow the natural development and possible separation of the forebody boundary layer, either of which influences, the flow at the engine inlets. The experimental results presented in Ref. 6 indicate that acceptable aerodynamic simulation is achieved when the static pressure distribution on the test body is within $\pm 10\%$ of that produced by an interference-free flowfield. This criterion is used in this study since it is probably adequate for most engine test programs. However, an acceptable criterion for jet stretcher performance should be based on the objectives of each specific test program.

For the test body static pressure distribution to be within $\pm 10\%$, the jet stretcher static pressure distribution must be within $\pm 5\%$ since a disturbance produced by the jet stretcher approximately doubles in magnitude when it strikes the test body. Therefore, the maximum acceptable angular misalignment between the jet stretcher and the interference-free flowfield (expressed as β in Fig. 14) can be estimated from the following equation for small disturbances:

$$\beta_{max} = \pm (0.05/\gamma M^2) (M^2 - 1)^{1/2} \quad (16)$$

Based on this equation, the maximum allowable angular misalignment of the jet stretcher varies from $\pm 0.886°$ to $\pm 0.56°$ in the Mach number range 2.0–3.5. Since this is a highly simplified analysis, a conservative value of $\pm 0.5°$ was used.

To summarize then, an axisymmetric jet stretcher designed for a fixed Mach number and zero angle of attack can be used for various other Mach numbers and finite angles of attack by locating the jet stretcher such that the local mismatch in angle (β Fig. 14) between the interference-free flowfield and the jet stretcher surface is within a prescribed tolerance. If this is not possible over the entire jet stretcher surface (that can influence the flowfield of interest) then only the jet stretcher inlet is matched within the prescribed tolerance. The remaining portions of the jet stretcher that exceed the prescribed tolerance can be corrected by making these surfaces porous and using bleed flow to reduce the disturbances.

The jet stretcher matching calculation for a finite test body angle of attack is greatly simplified by the previously mentioned experimental result that major disturbances originate from the top and bottom regions of jet stretcher while the sides remain acceptably matched to the interference-free flowfield. Therefore, if it is possible to acceptably match the top and bottom of the jet stretcher, then it is reasonable to assume that the entire jet stretcher surface is acceptably matched to the interference-free flowfield.

B. Experimental Jet Stretcher Performance

The same small-scale jet stretcher system used in the diffuser study was also used to verify the jet stretcher performance for test body angles of attack of 4° and 8°. However, the cylindrical diffuser was removed so that the jet stretcher ambient pressure (chamber pressure, p_c) could be controlled by the ETF exhaust plant.

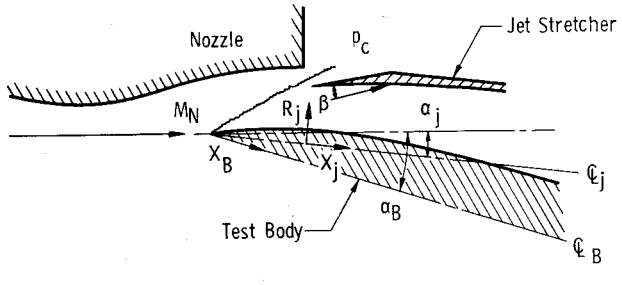

Fig. 14 Sketch showing jet stretcher mismatch angle β.

1. *Test body at 4° angle of attack*

The optimum position of the test body is that which allows the bow shock wave to pass through the edge of the nozzle exit boundary layer. This allows the jet stretcher to be located as close as possible to the nozzle exit in order to block undesirable disturbances from within the nozzle produced by a difference in pressure between the nozzle exit and the test cell, and thus, reduce diffuser requirements.

For this test configuration the test body was set near the optimum position by pitching the test body 4° about its nose from the zero angle-of-attack position as shown in Fig. 15. This was done for mechanical convenience since the optimum position would require translating the test body vertically by about 0.2 in. and horizontally by about 0.1 in. in order to correctly position the bow shock wave.

The optimum position of the jet stretcher was determined by computing the mismatch angle for various orientations of the jet stretcher. The interference-free flowfield was computed by the three-dimensional method of characteristics solution technique.[7] These results showed that the optimum position of the jet stretcher is obtained by pitching the jet stretcher about the nose of the test body through an angle of 1.5° from its design position at zero angle of attack. The region of jet stretcher influence on the test body is shown in Fig. 15. The mismatch angles β for the top and bottom of the jet stretcher are presented in Fig. 16. The results show that the top to the jet stretcher is acceptably matched over the entire length that

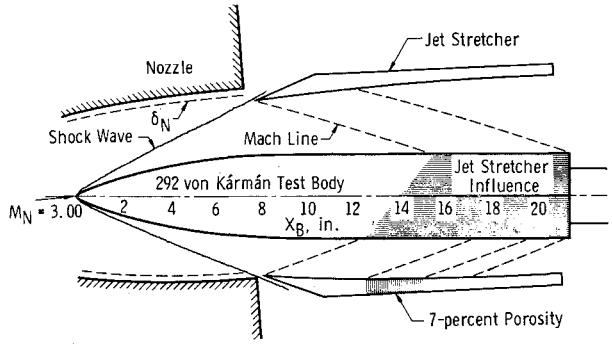

Fig. 15 Test configuration with test body at 4° and jet stretcher at 1.5° angles of attack.

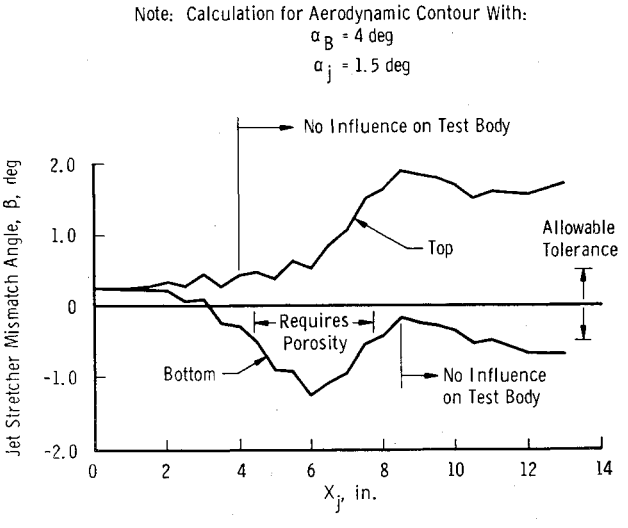

Fig. 16 Jet stretcher mismatch angle with test body at 4° and jet stretcher at 1.5° angles of attack.

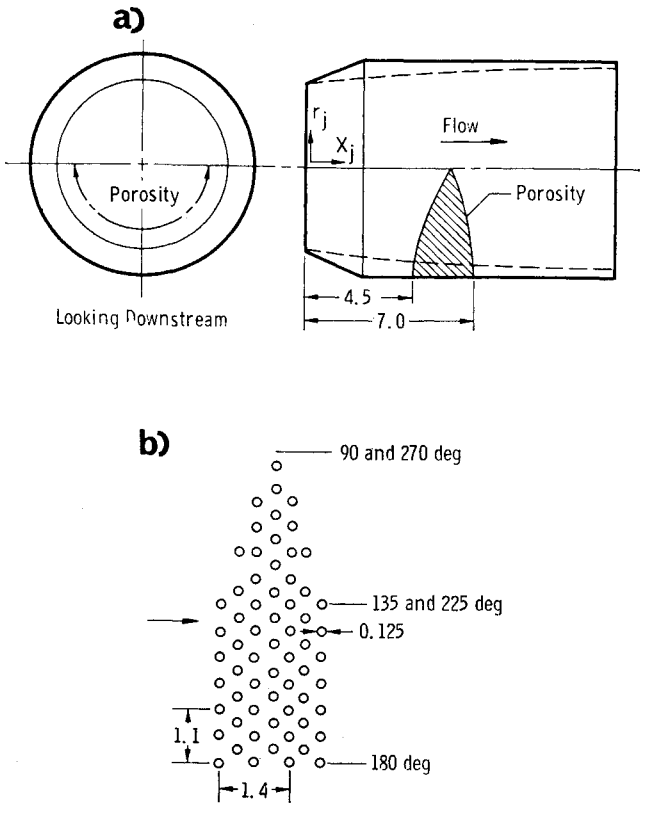

Fig. 17 Jet stretcher porosity; a) location of porosity; b) hole pattern.

can influence the test body. However, the bottom of the jet stretcher requires porosity in the region from station 4.4–7.7 in., and, since the mismatch angle is negative in this region, in-bleed is required.

The circumferential distribution of the porosity area on the jet stretcher surface was estimated by assuming a cosine variation in mismatch angle between the top and bottom of the jet stretcher. The location of the porosity area on the jet stretcher and the porosity hole pattern are presented in Figs. 17a and b.

The amount of porosity required for complete cancellation of the disturbance is a function of the local mismatch angle, β, the local pressure difference across the jet stretcher wall, and the corresponding characteristics of the porous wall. At the present time it is not possible to theoretically predict the characteristics of a porous wall with sufficient accuracy to obtain a realistic estimate of the required jet stretcher porosity. However, for the experimental apparatus used in this study it was possible to independently control the jet stretcher ambient pressure, and thus, control the pressure difference across the porous wall (bleed flow). Therefore, the amount of porosity was not a critical factor and a uniform hole pattern having approximately 7% porosity (open area to closed area) was used (Fig. 17b). Experimental results were obtained for various jet stretcher ambient pressure levels, and the optimum value was determined from the measured pressure distribution on the test body.

The experimental static pressure, distributions on the test model for roll angles θ of 0°, 90°, and 180° are presented in Figs. 18a–c. These experimental results with the jet stretcher are in good agreement with the corresponding results for interference-free flow. The influence of bleed flow through the porous region is shown in the pressure distribution on the windward side ($\theta = 180°$) of the test body. For small bleed flows ($p_c/p_N = 1.0$) an expansion wave disturbance occurs in the region requiring porosity as predicted by the theory. The optimum bleed flow occurs for a pressure ratio (p_c/p_N) of about 1.4

When testing in a full-scale test facility, the jet stretcher ambient pressure will be constant at a level determined by the exhaust diffuser performance. Consequently, the amount of porosity will be critical.

2. Test body at 8° angle of attack

For this test configuration, the near optimum location of the test body was obtained by pitching the test body about station 5 (5.0 in. aft of the nose) through an angle of 8° from its position in the zero angle-of-attack test configuration.

It was not possible to acceptably match the jet stretcher inlet to the interference-free flowfield. When the bottom of the jet stretcher was acceptably matched, the top of the jet

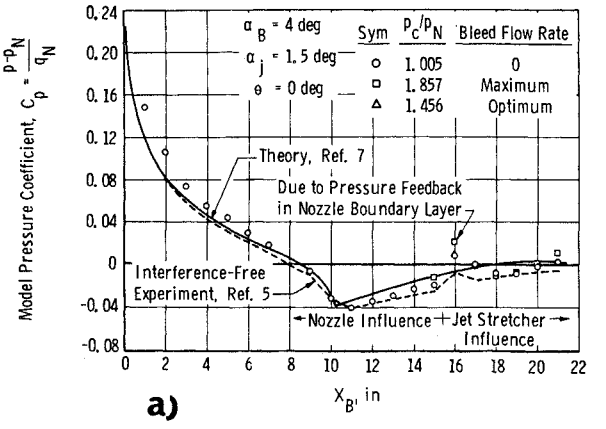

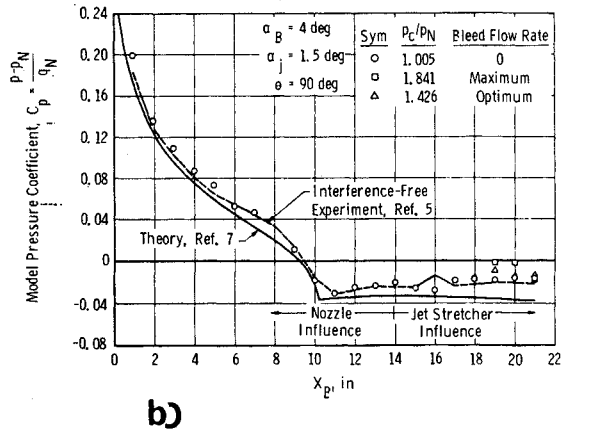

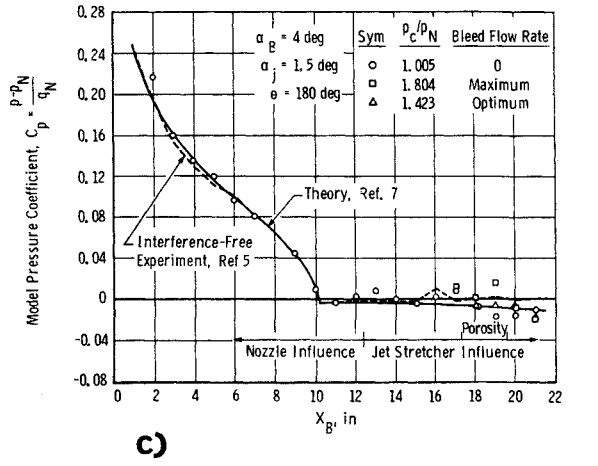

Fig. 18 Test body pressure distribution for 4° angle of attack; a)θ—0° (leeward side) b) θ—90°; c) θ—180° (windward side).

stretcher was at too steep an angle. However, the quality of the inlet flow at the bottom of the jet stretcher is much more influential than at the top so that a near optimum jet stretcher position is obtained by acceptably matching the bottom inlet of the jet stretcher. This was done by the following movements of the jet stretcher from its design position at zero angle of attack. First, the jet stretcher was translated vertically until its centerline passed through the nose of the test body after it was set at 8° angle of attack. Based on calculations to optimize the mismatch angle, β, the jet stretcher was pitched about the nose of the test body through an angle of 3.5°. The mismatch angles for the top and bottom of the jet stretcher are presented in Fig. 19. The mismatch angle, β, for the top of the jet stretcher varies from 1.2° to 1.6° over the length that can influence the flow over the test body. This angle exceeds the acceptable tolerance of $\pm$ 0.5° for aerodynamic testing and should produce undesirable compression disturbances. The bottom of the jet stretcher required porosity from station 3.7 in.–7.7 in. which is essentially the same region as that for testing at 4°-angle of attack. Therefore, the porosity pattern was not changed.

Experimental pressure distributions on the test body are compared with theory and experiment for interference-free flow in Figs. 20a–c, for corresponding roll angles θ of 0°, 90° and 180°. These results show that there are no major disturbances produced by the jet stretcher, not even by the top of the jet stretcher which did not match the established criteria for aerodynamic testing. The bottom of the jet stretcher is the most critical and the experimental results presented in Fig. 20c clearly show the expansion disturbance predicted by the theory. The porosity was located in the correct position to reduce this disturbance; however, the maximum chamber pressure ratio, p_c/p_N, of 1.4 allowed by this configuration did not produce enough bleed flow to be effective. This indicates that the amount of porosity should be increased.

Although the angle of attack limit of this test technique was exceeded with the test body at 8° angle of attack, the results suggest modifying the jet stretcher with wedge-shaped spacers. The purpose of the spacers is to rotate the top portion of the jet stretcher to obtain the desired aerodynamic matching. The use of spacers could significantly increase the angle of attack limit of this test technique.

VI. Conclusions

The major conclusions from this study are the following:

A. Diffuser Performance

1) The starting conditions of a jet stretcher diffuser system are determined by limitations imposed by the nozzle boundary layer, the test body blockage, and the chamber pressure. Analytical techniques were developed for estimating the starting conditions due to either the nozzle boundary layer or the chamber pressure. Experiments with the test body at zero angle of attack showed the accuracy of the boundary-layer analysis to be about 2% and the accuracy of the chamber pressure analysis to be about 10%.

2) With the test body at zero angle of attack, a cylindrical diffuser having a length to diameter ratio of 5.0 is sufficient for complete mixing. Experiments with the test body at an 8° angle of attack indicate that a longer diffuser is required.

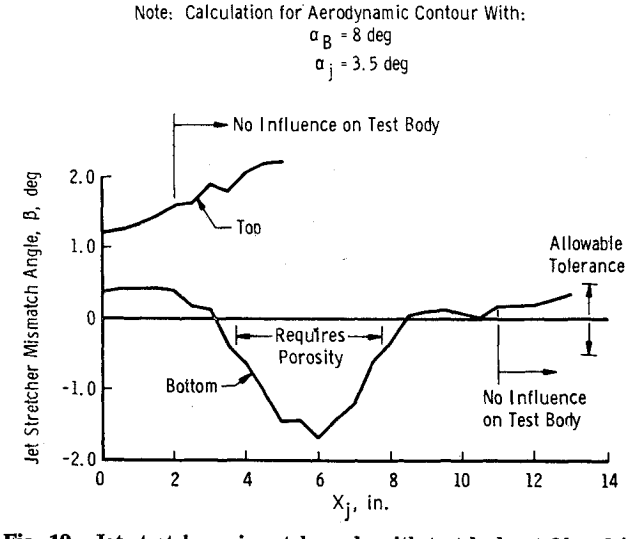

Fig. 19 Jet stretcher mismatch angle with test body at 8° and jet stretcher at 3.5 °angles of attack.

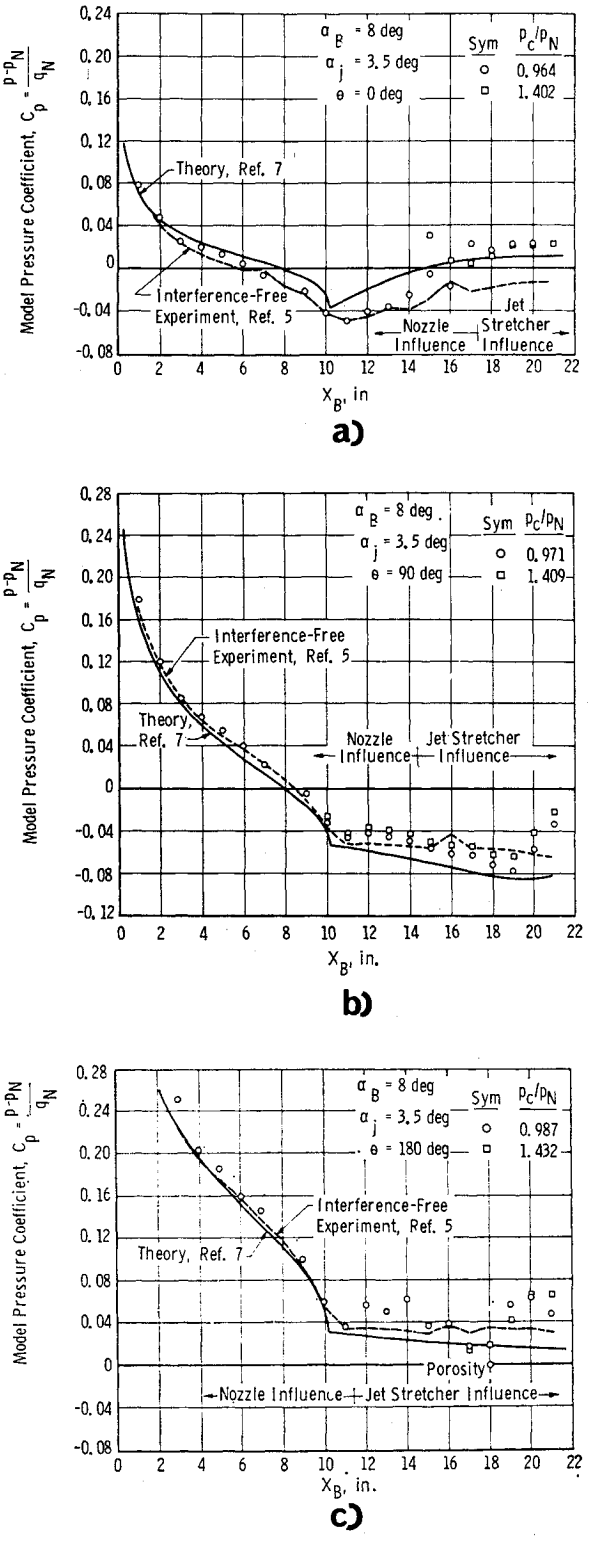

Fig. 20 Test body pressure distribution for 8° angle of attack.

3) Both test body angle of attack and closed engine inlets produce diffuser choking at an undesirably high chamber pressure. This choking cannot be analytically predicted at the present time.

4) The experimental results showed no hysteresis effects in that both the starting and operating conditions were identical.

B. Jet Stretcher Performance

1) By establishing an acceptable criteria for jet stretcher performance, it is possible to use an axisymmetric, porous jet stretcher in an off-design condition such as test body angle of attack. For the jet stretcher system considered the maximum possible off-design angle of attack of the test body is about 5.0° based on maintaining the test body static pressures to be within $\pm 10\%$.

2) The analytical technique for evaluating the off-design performance of a jet stretcher has been experimentally verified for angles of attack of 4° and 8°.

3) A significant improvement in the angle-of-attack capability of this testing technique can probably be achieved by modifying an axisymmetric jet stretcher with wedge-shaped spacers which increase the exit area of the jet stretcher.

4) Both the theory and experiment show that porosity is of secondary importance for these tests since the major disturbances were eliminated by properly positioning the jet stretcher However, when testing in a full-scale test facility, the jet stretcher ambient pressure will be constant at a level determined by the exhaust diffusers. Consequently, the amount of porosity will be critical.

References

[1] German, R. C., Armstrong, W. C., and Bauer, R. C., "A Study of the Jet Stretcher Concept," Presented at AIAA 6th Propulsion Joint Specialist Conference, San Diego, Calif. June 9–13, 1970.

[2] Weingold, H. D., "The ICRPG Turbulent Boundary Layer Reference Program," July 1968, Pratt and Whitney Aircraft, East Hartford, Conn.

[3] Schulz, R. J., "Rocket Exhaust Plumes in a Separated Supersonic External Stream," M.S. thesis, Dec. 1970, Dept. of Mechanical Engineering, Univ. of Tennessee, Space Institute, Tullahoma, Tenn.

[4] Zukoski, E. E., "Turbulent Boundary-Layer Separation in Front of a Forward Facing Step," *AIAA Journal*, Vol. 5, No. 10, Oct. 1967, pp. 1746–1753.

[5] German, R. C., "Simulation of Supersonic Flow over a Body of Revolution Using an Axisymmetric Jet Stretcher," AEDC–TR–70–166, Oct. 1970, Arnold Engineering Development Center, Arnold Air Force Station, Tenn.

[6] Barebo, R. L. and Matkins, E. C., "Simulation of Supersonic Flow over a Scale Model Missile with Aft-Mounted Inlets Using an Axisymmetric Jet Stretcher," AEDC–TR–71–37, AD514891, April 1971, Arnold Engineering Development Center, Arnold Air Force Station. Tenn.

[7] "The Addition of Secondary Shock Capability and Modification to the GASL Three Dimensional Characteristics Program," GASL Rept. 653, AD666742, Aug. 1967, General Applied Sciences Lab., Westbury, N. Y.